Reversible writing/deleting of magnetic skyrmions through hydrogen adsorption/desorption

Gong Chen (gchenncem@gmail.com)
Georgetown University
Colin Ophus
Lawrence Berkeley National Laboratory https://orcid.org/0000-0003-2348-8558
Alberto Quintana
Georgetown University https://orcid.org/0000-0002-9813-735X
Heeyoung Kwon
Korea Institute of Science and Technology
Changyeon Won
Kyung Hee University https://orcid.org/0000-0001-5987-7411
Haifeng Ding
Nanjing University https://orcid.org/0000-0001-7524-0779
Yizheng Wu
Fudan University https://orcid.org/0000-0002-9289-1271
Andreas Schmid
NCEM, Molecular Foundry, Lawrence Berkeley National Laboratory
Kai Liu
Georgetown University https://orcid.org/0000-0001-9413-6782

Article

Keywords: spintronics, magnetic skyrmions, magneto-ionic devices

Posted Date: June 23rd, 2021

DOI: https://doi.org/10.21203/rs.3.rs-575830/v1

Version of Record: A version of this preprint was published at Nature Communications on March 15th, 2022. See the published version at https://doi.org/10.1038/s41467-022-28968-4.

Abstract

Magnetic skyrmions are topologically nontrivial spin textures with envisioned applications in energy-efficient magnetic information storage. Toggling the presence of magnetic skyrmions via writing/deleting processes is essential for spintronics applications, which usually require the application of a magnetic or electric field or an electric current. Here we demonstrate the reversible field-free writing/deleting of skyrmions at room temperature, via hydrogen chemisorption/desorption on the surface of Ni and Co films. Supported by Monte-Carlo simulations, the skyrmion creation/annihilation is attributed to the hydrogen-induced magnetic anisotropy change on ferromagnetic surfaces. We also demonstrate the role of hydrogen and oxygen on magnetic anisotropy and skyrmion deletion on other magnetic surfaces. Our results open up new possibilities for designing skyrmionic and magneto-ionic devices.

Introduction

Magnetic skyrmions are bubble-like topological spin textures, characterized by a topological charge (or skyrmion number)[1,2]. One of the main mechanisms to stabilize skyrmions is the Dzyaloshinskii–Moriya interaction (DMI)[3,4]. The DMI only occurs under conditions where inversion symmetry is broken, for example in bulk B20 compounds[5] or in thin films[6], and skyrmions have been observed experimentally in many of these systems[2,7]. Due to their topologically protected spin configurations magnetic skyrmions have potential to be used as information carriers in spintronic applications, such as skyrmion-based memory[8,9], logic devices[10] or artificial neurons[11]. They may also find applications in more complex device architectures such as 3-dimensional (3D) racetrack memories[12] or interconnected networks[13]. Being able to create and annihilate skyrmions conveniently is a key step towards achieving skyrmion-based spintronic devices. So far, writing/deleting of skyrmions has been done primarily using an applied magnetic field, spin-polarized current injection[14-18], or applied electric field[19-21]. Recently, laser light pulses[22] and thermal excitation[23] have also been shown to generate skyrmions. Exploring new approaches to write/delete skyrmions, particularly in a contactless manner, is both fundamentally interesting and practically important for device applications.

Manipulating magnetic materials and structures with light elements such as hydrogen or oxygen is an effective way to tailor their properties in field-free conditions. For instance, hydrogen absorption has been used to alter magnetic properties in thin films, including magnetic moment[24], exchange coupling[25], and anisotropy[26]. It was also shown to prompt the formation of a magnetic skyrmion phase in the Fe/Ir(111) system in external magnetic fields at 4.2K [27]. In these prior observations, the altered magnetic properties were attributed to *absorption* of hydrogen into the bulk of the materials. On the other hand, *chemisorption* of hydrogen or oxygen on metal surfaces, limited to surface adsorption without penetrating into the metal interior[28], has been shown to induce DMI[29,30] and allow the tuning of magnetic anisotropy[31]. Understanding adsorbate induced magnetic properties is particularly relevant to the emerging field of magneto-ionics, where oxygen, hydrogen, or nitrogen ions can be driven to/from interfaces via electric fields, enabling the reversible tuning of magnetic properties such as magnetic anisotropy and magnetization[32-36]. Combining the exciting promise of skyrmion-based spintronics and

the field of light element-based magneto-ionics motivates the search for ways to control skyrmion properties through chemisorption.

In this paper, we report reversible hydrogen-driven writing/deleting of skyrmions in Ni/Co/Pd/W(110) multilayers at room temperature. Using spin polarized low energy electron microscopy (SPLEEM), skyrmion creation and annihilation is observed during hydrogen chemisorption / desorption cycles. We show that the adsorption of hydrogen on the surface of Ni/Co/Pd/W(110) multilayers changes the balance of magnetic energy contributions, particularly the magnetic anisotropy, which in turn drives the skyrmion creation/annihilation. Using SPLEEM for magnetization vector mapping we resolve the spin structure of the written skyrmions and show that they are left-handed hedgehog Néel-type. Monte-Carlo simulations support our interpretation attributing the reversible skyrmion writing and deleting to anisotropy changes. The roles of hydrogen and oxygen on magnetic anisotropy and skyrmion deletion on other magnetic surfaces are also demonstrated. Such ambient temperature reversible skyrmion operations in the absence of magnetic, electric field or electric current provide new paths for the design of skyrmion-based spintronics and magneto-ionic devices.

Hydrogen-induced reversible change of magnetic anisotropy and domain structure

One effective way to tailor magnetic domains is the control of magnetic anisotropy, especially near a spin reorientation transition (SRT), where domain patterns are very sensitive to small changes of magnetic anisotropy[37]. In our system of Ni/Co/Pd/W(110), the effective magnetic anisotropy can be tuned by adjusting the Ni layer thicknesses and, as long as the Co layer thickness is in the range of a few ML, two typical SRTs occur[38]. The first SRT from in-plane to out-of-plane appears with the deposition of a fraction of 1 monolayer (ML) of Ni, and the second SRT from out-of-plane to in-plane happens at a Ni thickness of about 2-3ML. Using SPLEEM, we start by observing the evolution of magnetic domain patterns as a function of Ni film thickness, where < 1ML (Fig. 1 a-d), which allows us to prepare samples near the first SRT. When Ni deposition is stopped right after the SRT, perpendicularly magnetized domains are observed in the test sample (Figs. 1d and 1e).

Chemisorbed hydrogen is subsequently added to the metal surface by dissociative adsorption of high-purity hydrogen leaked into the ultra-high vacuum chamber (Methods). Experimental studies[28,39] and density functional theory (DFT) calculations[40,41] have previously shown that the hydrogen atoms adsorb on the top surface and that diffusion into subsurface binding sites is thermodynamically hindered by the presence of a chemisorption energy well on both Ni and Co surfaces. On the fcc(111) - like Ni/Co surface, the hydrogen atoms are expected to occupy three-fold hollow sites, in the same binding geometry as on the close packed pure Ni[42] and Co surfaces[41]. The evolution of magnetic domains is monitored in real-time with the microscope aligned for out-of-plane magnetization sensitivity. Upon exposure of 0.7 Langmuir hydrogen, the out-of-plane magnetization component of the domains almost vanishes (Fig. 1h), indicating that chemisorbed hydrogen induces an in-plane anisotropy. Note that the surface only contains a fraction of a monolayer (0.3ML) of Ni, besides the chemisorption on the Ni, it is plausible to attribute the chemisorbed hydrogen induced in-plane anisotropy to the binding of hydrogen to the Co

sites. This is consistent with the observation of hydrogen adsorption induced in-plane anisotropy on Co/Ru(0001)[31], as well as with the in-plane anisotropy induced in the Pt/Co/GdO_x system via magneto-ionic proton transport[35].

Once the hydrogen flux is turned off, the domains gradually return to perpendicular magnetization as hydrogen desorbs at room temperature (Fig. 1i). The time-dependent evolution of out-of-plane magnetic contrast is plotted in Fig. 1j, showing the reversible hydrogen-induced anisotropy change during the chemisorption/desorption cycle. Note that the entire cycle occurs at room temperature without heating or cooling, which suggests that the magnitude of the binding energy of hydrogen on Ni/Co surfaces is in an experimentally convenient range[30,43]. Other systems where reversible control of magnetic anisotropy was realized by adsorption/desorption of hydrogen including Ni/Cu(001)[26] and Co/Ru(0001)[31] required heating for hydrogen desorption, which may trigger temperature-induced changes of the micromagnetic structure.

Writing a hedgehog skyrmion using hydrogen

The fact that chemisorbed hydrogen induces in-plane anisotropy on the Ni/Co surface allows us to tune the effective anisotropy near the SRT and therefore tailor the domain configurations in a controllable way (Fig. 2a). Magnetic films with perpendicular magnetic anisotropy (PMA) commonly form labyrinth (or stripe) domain structures near SRTs, which respond to changes of magnetic anisotropy by varying the domain width, i.e. the domain boundary density. Equilibrium phases composed of arrays of magnetic skyrmions (bubbles) are also possible, particularly under conditions where asymmetric $+\mathbf{M}_z$ and $-\mathbf{M}_z$ magnetized area fractions are stabilized either via external magnetic field, or via effective magnetic field from interlayer exchange coupling[44] or exchange bias[21], or in some cases without those driving forces (supplementary Fig. S1). In the Ni/Co/Pd/W(110) system, we have observed the evolution from in-plane magnetization to skyrmions (bubbles) during the film growth in the absence of magnetic field (supplementary Fig. S2). To demonstrate the hydrogen induced skyrmion creation, a domain that is out-of-plane magnetized with relatively weak PMA, i.e. close to SRT, is prepared by monitoring the magnetization using SPLEEM during Ni growth (Fig. 2b). Within this uniformly magnetized domain, during the exposure to 0.9 Langmuir hydrogen, a bubble-like domain appears (Fig. 2c).

Using SPLEEM we can image the three Cartesian components of the magnetization vector, thus mapping the spin-vector structures of domains in thin films[45]. Such a magnetization vector map is shown in the compound SPLEEM image (Fig. 2d). The black skyrmion core ($+\mathbf{M}_z$) within the grey out-of-plane magnetized domain ($-\mathbf{M}_z$) is surrounded by an in-plane magnetized skyrmion boundary where the local magnetization always points towards the core (see black arrows in Fig. 2d), showing that the observed bubble-like magnetic structure is a Néel-type skyrmion. For a statistically robust analysis of larger data sets, the angle between the domain boundary normal and the local magnetization vector is measured at all image pixels along the domain boundary[46]. Plotting histograms of this angle then permits unambiguous identification of the domain boundary chirality, as shown in Fig. 2e, where a single peak at confirms left-handed magnetic chirality. This chirality is determined by the effective DMI in the

Pd/W(110) system[29] where, as a result of opposite signs of the DMI at the Co/W (right-handed) and Co/Pd (left-handed) interfaces, the sign and the magnitude of the DMI can be tuned by adjusting the Pd film thickness . The thickness in this sample is much larger than the zero-DMI thickness where the left-handed DMI of Pd just compensates the right-handed DMI of the W(110) substrate, therefore the effective DMI in this sample is Pd-like, i.e. left-handed. To display the measured spin structure more clearly, the same image is plotted again in Fig. 2f as an arrows array, where the orientations of the arrows represent the magnetization directions measured at image pixels in the central region of panel 2d, highlighting the experimentally measured spin structure of this hedgehog skyrmion.

Writing and deleting of skyrmions using hydrogen

Observation of the reversible control of magnetic anisotropy via hydrogen chemisorption/desorption, as summarized in Fig. 1, together with the hydrogen-induced writing of skyrmions, as shown in Fig. 2, suggests the opportunity of creating/annihilating skyrmions via cycles of hydrogen chemisorption/desorption. A sample of Ni/Co/Pd/W(110) with weak PMA and some initial skyrmions was prepared, and Fig. 3a shows the evolution of its magnetization within a -$\mathbf{M}_z$ domain over three hydrogen ON/OFF cycles, where skyrmions are created in each H-ON state and annihilated in each H-OFF state. The total dose for each H-ON cycle is 0.9L ($5x10^{-9}$ torr hydrogen for 3 minutes). The duration of the hydrogen OFF cycles was chosen to be sufficiently long to allow spontaneous room temperature desorption of the hydrogen and recovery of the magnetization to nearly its original state. The hydrogen desorption rate, being a function of the hydrogen binding energy to the Ni/Co/Pd/W surface, is somewhat dependent on the sub-monolayer Ni film thickness [30,43]. We find that the skyrmions are mostly created/deleted at the same location on the film surface, which is likely related to small variations of anisotropy across the film. We speculate that the exact value of the PMA has fluctuations associated with details of atomic-scale surface and interface properties such as defects and step density,[47] and that areas featuring slightly reduced PMA may result in higher probability for skyrmion creation; this hypothesis was tested in Monte-Carlo simulations described below. There are also some skyrmions already present prior to the introduction of hydrogen, which are not sensitive to hydrogen. We also show equivalent hydrogen ON/OFF cycles on a domain magnetized in the opposite direction, +$\mathbf{M}_z$ (Fig. 3b), where similar skyrmion switching is observed. Successful skyrmion switching on both +$\mathbf{M}_z$ and -$\mathbf{M}_z$ domains excludes any unidirectional driving force, such as magnetic field.

The creation and annihilation times of these individual skyrmions were extracted from the microscopy data in Figs. 3a and 3b, and plotted in Fig. 3c. The measurable differences in the exact time at which individual skyrmions are turned on and off are likely related to the hypothesized landscape of PMA variations, and possibly to hydrogen adsorption/desorption rate variations associated with microscopic variations of the Ni coverage. To measure the size of the skyrmions based on their magnetization profiles (Fig. 3d), we follow Ref. [48] and start by assuming that observed skyrmion images represent convolutions of the skyrmions' physical magnetization profiles and the resolution limit of the SPLEEM images. The instrumental blur is evident by observing how the regions of reversed magnetization in the skyrmion cores are clearly resolved in larger skyrmions and is progressively blurred as skyrmion size

declines. Fig. 3d shows an example of this deconvolution, where the red solid curve represents the apparent skyrmion profile as measured directly from the image and the blue dashed curve represents the estimate of its physical size based on deconvoluting the image blur. Histograms of skyrmion sizes measured during three write/delete cycles are shown in Fig 3e, where the lower scale indicates apparent diameters from the images and the upper scale, labeled 'deconvoluted diameter', represents the results including deconvolution of image blur. These data indicate that the average diameter of these ensembles of skyrmions is of the order of 100nm, with many skyrmions in the sub-100nm size region. No significant correlation between the skyrmion diameter and the writing or deleting time is observed (Supplementary Fig. S3). We note that theoretical modeling of similar PMA systems predicts that the response of domain patterns to anisotropy changes is expected to result in variation of the width of stripe domains[49], while bubble domains are favoured when the degeneracy of $+\mathbf{M}_z$ vs. $-\mathbf{M}_z$ magnetization is broken by a unidirectional driving force. This general picture suggests that a rich variety of additional applications of the hydrogen-induced skyrmion writing/deleting could be realized by adding applied fields or by introducing interlayer exchange coupling[44] or exchange bias[21].

Monte-Carlo simulation

Monte-Carlo simulations were performed to further understand the skyrmion writing/deleting process (see Methods). To simulate an out-of-plane magnetized film that is close to a SRT, an out-of-plane magnetized domain is initialized with small PMA K_z=+0.4. In addition, eleven pinning regions are simulated by locally reducing PMA in the range of 0.35 to 0.15 in steps of 0.02 (Fig. 4a). The role of the hydrogen chemisorption is simulated as a negative magnetic anisotropy shift of -0.10 on the entire area. The simulation shows that hydrogen chemisorption (i.e. anisotropy shift by -0.10) results in the creation of skyrmions at the pinning sites where K_z ranges from 0.29 to 0.19. At the regions with the lowest anisotropy (K_z=0.17 and 0.15 in Fig. 4b) skyrmions remain stable with or without the simulated hydrogen adsorption. Because the chemisorbed hydrogen does not always fully desorb on the Ni/Co surface[30], a partial recovery of magnetic anisotropy by +0.08 within the finite H-OFF time (Fig. 1j) was simulated, which showed that only those skyrmions with K_z=0.29, 0.27, 0.25 and 0.23 were deleted. Additional cycles of anisotropy changes, varying the anisotropy by -0.08 (mimicking H-ON) and +0.08 (H-OFF), reproduce the reversible writing and deleting of skyrmions as was observed in the experiment (Fig. 3a). The simulations are summarized in Fig. 4c by plotting skyrmion presence (grey circles) and absence (open circles) in anisotropy versus H-cycle space, showing that the skyrmion switching occurs once the effective magnetic anisotropy crosses a boundary near K_z=+0.2 in the energy landscape between the two phases.

Possible writing/deleting of skyrmions in other systems

The simulation results suggest that writing/deleting of skyrmions via chemisorption-induced anisotropy may be a general approach. Thus it is useful to explore skyrmion writing/deleting in other systems as well, particularly in light of potential hydrogen and oxygen based applications in magneto-ionics[32-35]. Chemisorption of hydrogen occurs on surfaces of other metals[28], e.g. on the Ni(111). Fig. 5a shows the

evolution of spin structures including skyrmions during hydrogen chemisorption on the surface of 2ML Ni/3ML Co/Pd/W(110), where the chemisorption is comparable to the bulk-Ni(111) case because of the much thicker Ni film [30], in contrast to that shown in Figs. 1-3. It is interesting to point out that while chemisorbed hydrogen induces in-plane magnetic anisotropy on the Co-rich surface (see also the same trend on the close-packed Co surface in Co/Ru(0001)[31], chemisorbed hydrogen *enhances* the PMA on the Ni(111) surface. Chemisorption of oxygen also occurs on Ni and Co surfaces[29]. Here we test the role of oxygen chemisorption on a Co-rich surface in a 0.3 ML Ni/3ML Co/Pd/W(110) sample, and on a pure Ni surface in a 2ML Ni/3ML Co/Pd/W(110) sample. We find that chemisorbed oxygen *enhances* the PMA in both the Co-rich and the Ni surfaces. In these three cases, we demonstrate that magnetic skyrmions can be *deleted* upon chemisorption (Fig. 5 insets) as a result of the greater PMA of the system, which is opposite to the case of hydrogen on Co-rich surface (Figs. 1-3). Note that in these cases we have not observed reversibility of skyrmion formation, partly as a result of kinetically less favourable conditions due to higher binding energies between adsorbates and surfaces. However, reversible skyrmion switching may be facilitated via magneto-ionic approaches, e.g., using an electric field,[35] as discussed further below.

The writing/deleting of magnetic skyrmions via adsorption/desorption adds a new degree of freedom to chiral spintronics, where spin textures may be controlled in a tunable and contactless way, without the need for electrical leads. This may be particularly relevant for three-dimensional information storage schemes involving complex architectures and large numbers of skyrmions, such as racetrack memories[12] or interconnected networks[13]. This effect can also be readily integrated into magneto-ionic devices consisting of ferromagnet/reservoir heterostructures, where the adsorption/desorption takes place at buried interfaces.[35] For example, oxygen, hydrogen or other species may be stored in a reservoir layer, and subsequently driven into contact with a ferromagnetic layer, where chemisorption/desorption may occur at the ferromagnet/reservoir interface. It would be particularly attractive to reversibly control the magnetic anisotropy and interfacial DMI via chemisorption, and in turn skyrmion writing/deleting, especially given the high mobility of hydrogen in solids. Note that the essential adsorption/desorption processes may occur at the relevant ferromagnet interface with the reservoir layer, without penetrating inside the ferromagnet, thus enabling reversibility. In this case high switching speeds reaching < 1ns[50] may be possible, as the ionic species only need to traverse atomic distances to trigger chemisorption/desorption under proper device design. Such skyrmion based devices with magneto-ionic functionality may be used for magnetic memory and logic devices, as well as artificial synapses.

Conclusions

In summary, we report the writing/deleting of skyrmion via hydrogen chemisorption/desorption on the surface of ferromagnets at room temperature, in the absence of magnetic / electric field or electric current. Magnetization vector imaging by SPLEEM shows that the hydrogen chemisorption induced skyrmions are of the hedgehog Néel-type and the diameter of the skyrmions can be down to sub-100 nm. The driving force is attributed to hydrogen chemisorption induced magnetic anisotropy changes, which is supported by Monte-Carlo simulations. We also explore extension of the mechanism to chemisorbed

hydrogen and oxygen on both Ni and Co-rich surfaces. These results open up alternative approaches for designing skyrmion-based devices.

Methods

Sample preparation. The experiments were performed at the National Center for Electron Microscopy of the Lawrence Berkeley National Laboratory. Samples were grown under ultra-high vacuum conditions in the SPLEEM chamber, with a base pressure better than 4.0×10^{-11} torr. The W(110) substrate was prepared by cycles of flashing to 1,950 in 3.0×10^{-8} torr oxygen until the surface was free of carbon, followed by a final flashing at the same temperature to remove oxygen. Ni, Co and Pd layers were deposited by means of physical vapor deposition from electron beam evaporators, while the substrate is held at room temperature. The film thicknesses of the metal layers were calibrated via oscillations of the LEEM intensity associated with layer-by-layer growth[29]. Hydrogen exposures were introduced by leaking hydrogen of 99.999% purity at a pressure of into the SPLEEM chamber. The reading of the hydrogen pressure on the ionization gauge was corrected by a factor of 0.46.

Magnetic imaging and analysis. The real-space magnetic images were taken using the SPLEEM at the National Center for Electron Microscopy of the Lawrence Berkeley National Laboratory. The magnetic contrast is the asymmetry A of the spin-dependent reflectivities I between spin-polarized beams with up ( ) and down ( ) polarization, . This asymmetry A is proportional to , where **P** is the spin polarization vector of the illumination electron beam and **M** is the magnetization vector. Therefore the Cartesian components M_x, M_y and M_z of the magnetization can be obtained by setting the spin-polarization alignment along the x, y, z directions, respectively[45]. The energies of the incident electron beam were set to a value in the range of 5-6eV to optimize the magnetic contrast for the Ni/Co/Pd/W(110) system with various film thicknesses. All images were measured with the samples held at room temperature.

Image drift-correction and denoising are applied on time-dependent SPLEEM image sequences. The estimation of the deconvoluted skyrmion profile is described in ref. [48], and we use full-width-at-half-maximum of the skyrmion profile as the skyrmion diameter for both image-apparent and deconvoluted values. The compound SPLEEM images are converted by combining three sets of M_x, M_y and M_z SPLEEM images, where the colour wheel represents in-plane magnetization directions, and grey values indicate the perpendicular magnetization component $+M_z$ (black), $-M_z$ (grey), respectively. The method to analyze the magnetic chirality from the SPLEEM images is described previously[46].

The time series data were analyzed using custom Matlab codes with three pre-processing steps. Histograms of the measured intensity were used to fit scaling coefficients to the $\mathbf{M}_z$ channel, such that the two domains had mean values of -1 and +1, and then applied this scaling to all images. Next, cross correlation was used to align the windowed images, and applied the measured shifts to all images. Finally, a moving median filter was used to produce a denoised time series in order to better identify candidate skyrmion locations.

Next, the spatial and temporal behaviour of the skyrmion signals were analyzed. First, a Hough transform consisting of a 2D Gaussian shape (normalized by subtracting an error function profile to give the kernel a mean value of zero) was applied to each of the images, with a large range of radii. From the local maxima of the Hough transform over space global maxima as well as over time, we selected candidate skymion signals. We then fit a 2D Gaussian distribution to each of these candidates, over all time points. We used the scaling prefactor of the 2D Gaussian to identify skyrmions "turned ON" and "turned OFF," i.e. which had prefactors that initially started near 0, then rose above +0.5 (or fell below -0.5 in the other domain), then fell back to near 0. From this subset of the skyrmions, we computed the diameter, the time between H ON and skyrmion creation, and the time between H OFF and skyrmion annihilation.

Monte-Carlo Simulations

The Monte Carlo simulations were carried out based on a two-dimensional model, where exchange interaction, magnetic anisotropy, and the DMI are considered. The Hamiltonian is written as:

$$\mathcal{H} = -J \sum_{<i,j>} \mathbf{S}_i \cdot \mathbf{S}_j - \sum_{<i,j>} \boldsymbol{\beta}_{ij} \cdot (\mathbf{S}_i \times \mathbf{S}_j) - K_z \sum_i \left|\mathbf{S}_{i,z}\right|^2$$

where $\mathbf{S}_i$ and $\mathbf{S}_j$ are spins located on sites i and j in a two-dimensional square lattice system. The dimensionless parameters J, β, K_z correspond to exchange interaction, DMI, magnetic anisotropy, respectively. To focus on the local switching behaviors of the skyrmions shown in our experiments, dipolar interaction is simply approximated as a shape anisotropy form. Thus, K_z can be considered as an effective anisotropy defined by the competition between the crystalline anisotropy of the system and the shape anisotropy induced by the dipolar interaction. Domain configurations shown in Fig. 4 are simulated using 1000×100 lattice sites with periodic boundary condition applied for all directions (the centre 1000×50 area is shown in the figure), with the values of $J = 1$, $\beta = 0.3$, and $K_z = 0.40$ (initial state), 0.30 (H ON state), 0.38 (H OFF state). Eleven anisotropy defect sites with various K_z are placed in the highlighted area in Fig. 4a, where $K_{z,site}$ are weaken by $\Delta K_{z,site} = -0.05$ to -0.25 with a step of 0.02. The diameter of these circle-like defects is 10 lattice sites. System temperature is applied by allowing spin fluctuations according to Boltzmann statistics. For each H ON or H OFF states, 100,000 iterations are performed to make the total energy stabilized, and the averaged spin configurations in the last 5000 iterations are shown in each cycle in Fig. 4.

Declarations

ACKNOWLEDGMENTS

We are grateful to Professor Gen Yin for helpful discussions. This work has been supported by the NSF (DMR-2005108), and in part by SMART (2018-NE-2861), one of seven centers of nCORE, a Semiconductor Research Corporation program, sponsored by the National Institute of Standards and Technology (NIST). Work at the Molecular Foundry was supported by the Office of Science, Office of Basic Energy Sciences, of the US Department of Energy under contract no. DE-AC02-05CH11231. CO acknowledges support from the U.S. Department of Energy Early Career Research Program. HK acknowledges the support by Basic

Science Research Program through the National Research Foundation of Korea (NRF) funded by the Ministry of Education (NRF-2019R1A6A3A01091209). CW acknowledges the support by Grants from the National Research Foundation of Korea, funded by the Korean Government (NRF-2018R1D1A1B07047114). HFD acknowledges the support by the National Key R&D Program of China (grants no. 2017YFA0303202); the National Natural Science Foundation of China (grants no. 11974165 and no. 11734006).

Author contributions

G.C. and K.L. conceived the study and coordinated the project. G.C. carried out the experiments. A.K.S. supervised the SPLEEM facility. G.C. and C.O. analyzed the imaging data. H.K. and C.W. performed Monte-Carlo simulation. G.C., A.Q., H.D., Y.W., A.K.S. and K.L. discussed and interpreted the results. G.C., A.K.S. and K.L. prepared the manuscript. All authors contributed to the manuscript revision.

Additional information

Competing interests: Chen, Schmid, and Liu are co-inventors of a pending patent application on the large Dzyaloshinskii-Moriya interaction induced by chemisorbed species on ferromagnets that relates to this work.

References

[1] A. Fert, V. Cros, and J. Sampaio, *Skyrmions on the track*. Nat Nanotechnol **8**, 152 (2013).

[2] N. Nagaosa and Y. Tokura, *Topological properties and dynamics of magnetic skyrmions*. Nat. Nanotechnol. **8**, 899 (2013).

[3] I. Dzyaloshinsky, *A Thermodynamic Theory of Weak Ferromagnetism of Antiferromagnetics*. J. Phys. Chem. Solids **4**, 241 (1958).

[4] T. Moriya, *Anisotropic Superexchange Interaction and Weak Ferromagnetism*. Phys. Rev. **120**, 91 (1960).

[5] M. Uchida, Y. Onose, Y. Matsui, and Y. Tokura, *Real-space observation of helical spin order*. Science **311**, 359 (2006).

[6] M. Bode, M. Heide, K. von Bergmann, P. Ferriani, S. Heinze, G. Bihlmayer, A. Kubetzka, O. Pietzsch, S. Blugel, and R. Wiesendanger, *Chiral magnetic order at surfaces driven by inversion asymmetry*. Nature **447**, 190 (2007).

[7] W. Jiang, G. Chen, K. Liu, J. Zang, S. G. E. te Velthuis, and A. Hoffmann, *Skyrmions in magnetic multilayers*. Phys. Rep. **704**, 1 (2017).

[8] J. Iwasaki, M. Mochizuki, and N. Nagaosa, *Current-induced skyrmion dynamics in constricted geometries*. Nat Nanotechnol **8**, 742 (2013).

[9] J. Sampaio, V. Cros, S. Rohart, A. Thiaville, and A. Fert, *Nucleation, stability and current-induced motion of isolated magnetic skyrmions in nanostructures*. Nat Nanotechnol **8**, 839 (2013).

[10] X. C. Zhang, M. Ezawa, and Y. Zhou, *Magnetic skyrmion logic gates: conversion, duplication and merging of skyrmions*. Sci. Rep. **5**, 9400 (2015).

[11] K. M. Song, J.-S. Jeong, B. Pan, X. Zhang, J. Xia, S. Cha, T.-E. Park, K. Kim, S. Finizio, J. Raabe, J. Chang, Y. Zhou, W. Zhao, W. Kang, H. Ju, and S. Woo, *Skyrmion-based artificial synapses for neuromorphic computing*. Nat. Electron. **3**, 148 (2020).

[12] S. Parkin and S.-H. Yang, *Memory on the racetrack*. Nat. Nano. **10**, 195 (2015).

[13] E. C. Burks, D. A. Gilbert, P. D. Murray, C. Flores, T. E. Felter, S. Charnvanichborikarn, S. O. Kucheyev, J. D. Colvin, G. Yin, and K. Liu, *3D Nanomagnetism in Low Density Interconnected Nanowire Networks*. Nano Lett. **21**, 716−722 (2021).

[14] N. Romming, C. Hanneken, M. Menzel, J. E. Bickel, B. Wolter, K. von Bergmann, A. Kubetzka, and R. Wiesendanger, *Writing and deleting single magnetic skyrmions*. Science **341**, 636 (2013).

[15] W. J. Jiang, P. Upadhyaya, W. Zhang, G. Q. Yu, M. B. Jungfleisch, F. Y. Fradin, J. E. Pearson, Y. Tserkovnyak, K. L. Wang, O. Heinonen, S. G. E. te Velthuis, and A. Hoffmann, *Blowing magnetic skyrmion bubbles*. Science **349**, 283 (2015).

[16] D. A. Gilbert, B. B. Maranville, A. L. Balk, B. J. Kirby, P. Fischer, D. T. Pierce, J. Unguris, J. A. Borchers, and K. Liu, *Realization of Ground State Artificial Skyrmion Lattices at Room Temperature*. Nat. Commun. **6**, 8462 (2015).

[17] S. Woo, K. Litzius, B. Kruger, M. Y. Im, L. Caretta, K. Richter, M. Mann, A. Krone, R. M. Reeve, M. Weigand, P. Agrawal, I. Lemesh, M. A. Mawass, P. Fischer, M. Klaui, and G. S. Beach, *Observation of room-temperature magnetic skyrmions and their current-driven dynamics in ultrathin metallic ferromagnets*. Nat. Mater. **15**, 501 (2016).

[18] F. Buttner, I. Lemesh, M. Schneider, B. Pfau, C. M. Gunther, P. Hessing, J. Geilhufe, L. Caretta, D. Engel, B. Kruger, J. Viefhaus, S. Eisebitt, and G. S. D. Beach, *Field-free deterministic ultrafast creation of magnetic skyrmions by spin-orbit torques*. Nat. Nanotechnol. **12**, 1040 (2017).

[19] P. J. Hsu, A. Kubetzka, A. Finco, N. Romming, K. von Bergmann, and R. Wiesendanger, *Electric-field-driven switching of individual magnetic skyrmions*. Nat. Nanotechnol. **12**, 123 (2017).

[20] C. Ma, X. C. Zhang, J. Xia, M. Ezawa, W. J. Jiang, T. Ono, S. N. Piramanayagam, A. Morisako, Y. Zhou, and X. X. Liu, *Electric Field-Induced Creation and Directional Motion of Domain Walls and Skyrmion*

Bubbles. Nano Lett. **19**, 353 (2019).

[21] D. Bhattacharya, S. A. Razavi, H. Wu, B. Dai, K. L. Wang, and J. Atulasimha, *Creation and annihilation of non-volatile fixed magnetic skyrmions using voltage control of magnetic anisotropy*. Nat. Electron. **3**, 539 (2020).

[22] G. Berruto, I. Madan, Y. Murooka, G. M. Vanacore, E. Pomarico, J. Rajeswari, R. Lamb, P. Huang, A. J. Kruchkov, Y. Togawa, T. LaGrange, D. McGrouther, H. M. Ronnow, and F. Carbone, *Laser-Induced Skyrmion Writing and Erasing in an Ultrafast Cryo-Lorentz Transmission Electron Microscope*. Phys. Rev. Lett. **120** (2018).

[23] Z. D. Wang, M. H. Guo, H. A. Zhou, L. Zhao, T. Xu, R. Tomasello, H. Bai, Y. Q. Dong, S. G. Je, W. L. Chao, H. S. Han, S. Lee, K. S. Lee, Y. Y. Yao, W. Han, C. Song, H. Q. Wu, M. Carpentieri, G. Finocchio, M. Y. Im, S. Z. Lin, and W. J. Jiang, *Thermal generation, manipulation and thermoelectric detection of skyrmions*. Nat. Electron. **3**, 672 (2020).

[24] G. J. Mankey, M. T. Kief, F. Huang, and R. F. Willis, *Hydrogen Chemisorption on Ferromagnetic Thin-Film Surfaces*. J. Vac. Sci. Technol. **11**, 2034 (1993).

[25] B. Hjorvarsson, J. A. Dura, P. Isberg, T. Watanabe, T. J. Udovic, G. Andersson, and C. F. Majkrzak, *Reversible tuning of the magnetic exchange coupling in Fe/V (001) superlattices using hydrogen*. Phys. Rev. Lett. **79**, 901 (1997).

[26] D. Sander, W. Pan, S. Ouazi, J. Kirschner, W. Meyer, M. Krause, S. Muller, L. Hammer, and K. Heinz, *Reversible H-induced switching of the magnetic easy axis in Ni/Cu(001) thin films*. Phys. Rev. Lett. **93**, 247203 (2004).

[27] P. J. Hsu, L. Rozsa, A. Finco, L. Schmidt, K. Palotas, E. Vedmedenko, L. Udvardi, L. Szunyogh, A. Kubetzka, K. von Bergmann, and R. Wiesendanger, *Inducing skyrmions in ultrathin Fe films by hydrogen exposure*. Nat. Commun. **9**, 1571 (2018).

[28] K. Christmann, *Interaction of Hydrogen with Solid-Surfaces*. Surf Sci Rep **9**, 1 (1988).

[29] G. Chen, A. Mascaraque, H. Jia, B. Zimmermann, M. Robertson, R. L. Conte, M. Hoffmann, M. A. González Barrio, H. Ding, R. Wiesendanger, E. G. Michel, S. Blügel, A. K. Schmid, and K. Liu, *Large Dzyaloshinskii-Moriya interaction induced by chemisorbed oxygen on a ferromagnet surface*. Sci. Adv. **6**, eaba4924 (2020).

[30] G. Chen, M. Robertson, M. Hoffmann, C. Ophus, A. L. F. Cauduro, R. Lo Conte, H. F. Ding, R. Wiesendanger, S. Blügel, A. K. Schmid, and K. Liu, *Observation of hydrogen-induced Dzyaloshinskii-Moriya interaction and reversible switching of magnetic chirality*. Phys. Rev. X **11**, 021015 (2021).

[31] B. Santos, S. Gallego, A. Mascaraque, K. F. McCarty, A. Quesada, A. T. N'Diaye, A. K. Schmid, and J. de la Figuera, *Hydrogen-induced reversible spin-reorientation transition and magnetic stripe domain*

phase in bilayer Co on Ru(0001). Phys. Rev. B **85**, 134409 (2012).

[32] U. Bauer, L. Yao, A. J. Tan, P. Agrawal, S. Emori, H. L. Tuller, S. van Dijken, and G. S. D. Beach, *Magneto-ionic control of interfacial magnetism*. Nat. Mater. **14**, 174 (2015).

[33] D. A. Gilbert, J. Olamit, R. K. Dumas, B. J. Kirby, A. J. Grutter, B. B. Maranville, E. Arenholz, J. A. Borchers, and K. Liu, *Controllable Positive Exchange Bias via Redox-Driven Oxygen Migration*. Nat. Commun. **7**, 11050 (2016).

[34] D. A. Gilbert, A. J. Grutter, E. Arenholz, K. Liu, B. J. Kirby, J. A. Borchers, and B. B. Maranville, *Structural and magnetic depth profiles of magneto-ionic heterostructures beyond the interface limit*. Nat. Commun. **7**, 12264 (2016).

[35] A. J. Tan, M. Huang, C. O. Avci, F. Büttner, M. Mann, W. Hu, C. Mazzoli, S. Wilkins, H. L. Tuller, and G. S. D. Beach, *Magneto-ionic control of magnetism using a solid-state proton pump*. Nat. Mater. **18**, 35 (2019).

[36] J. de Rojas, A. Quintana, A. Lopeandia, J. Salguero, B. Muniz, F. Ibrahim, M. Chshiev, A. Nicolenco, M. O. Liedke, M. Butterling, A. Wagner, V. Sireus, L. Abad, C. J. Jensen, K. Liu, J. Nogues, J. L. Costa-Kramer, E. Menendez, and J. Sort, *Voltage-driven motion of nitrogen ions: a new paradigm for magneto-ionics*. Nature Communications **11**, 5871 (2020).

[37] Y. Z. Wu, C. Won, A. Scholl, A. Doran, H. W. Zhao, X. F. Jin, and Z. Q. Qiu, *Magnetic stripe domains in coupled magnetic sandwiches*. Phys. Rev. Lett. **93**, 117205 (2004).

[38] C. Won, Y. Z. Wu, J. Choi, W. Kim, A. Scholl, A. Doran, T. Owens, J. Wu, X. F. Jin, H. W. Zhao, and Z. Q. Qiu, *Magnetic stripe melting at the spin reorientation transition inFe/Ni/Cu(001)*. Phys. Rev. B **71** (2005).

[39] I. Chorkendorff, J. N. Russell, and J. T. Yates, *Hydrogen Implantation in Ni(111) - a Study of H-2 Desorption Dynamics from the Bulk*. Surf. Sci. **182**, 375 (1987).

[40] B. Bhatia and D. S. Sholl, *Chemisorption and diffusion of hydrogen on surface and subsurface sites of flat and stepped nickel surfaces*. J. Chem. Phys. **122**, 204707 (2005).

[41] J. Greeley and M. Mavrikakis, *Surface and subsurface hydrogen: Adsorption properties on transition metals and near-surface alloys*. J. Phys. Chem. B **109**, 3460 (2005).

[42] K. Christmann, R. J. Behm, G. Ertl, M. A. Van Hove, and W. H. Weinberg, *Chemisorption geometry of hydrogen on Ni(111): Order and disorder*. J. Chem. Phys. **70**, 4168 (1979).

[43] J. Greeley, T. F. Jaramillo, J. Bonde, I. Chorkendorff, and J. K. Nørskov, *Computational high-throughput screening of electrocatalytic materials for hydrogen evolution*. Nat. Mater. **5**, 909 (2006).

[44] G. Chen, A. Mascaraque, A. T. N'Diaye, and A. K. Schmid, *Room temperature skyrmion ground state stabilized through interlayer exchange coupling*. Appl. Phys. Lett. **106** (2015).

[45] G. Chen, J. Zhu, A. Quesada, J. Li, A. T. N'Diaye, Y. Huo, T. P. Ma, Y. Chen, H. Y. Kwon, C. Won, Z. Q. Qiu, A. K. Schmid, and Y. Z. Wu, *Novel chiral magnetic domain wall structure in Fe/Ni/Cu(001) films*. Phys. Rev. Lett. **110**, 177204 (2013).

[46] G. Chen, T. Ma, A. T. N'Diaye, H. Kwon, C. Won, Y. Wu, and A. K. Schmid, *Tailoring the chirality of magnetic domain walls by interface engineering*. Nat. Commun. **4**, 2671 (2013).

[47] J. E. Davies, O. Hellwig, E. E. Fullerton, G. Denbeaux, J. B. Kortright, and K. Liu, *Magnetization reversal of Co/Pt multilayers: Microscopic origin of high-field magnetic irreversibility*. Phys. Rev. B **70**, 224434 (2004).

[48] C. Moreau-Luchaire, S. C. Mouta, N. Reyren, J. Sampaio, C. A. Vaz, N. Van Horne, K. Bouzehouane, K. Garcia, C. Deranlot, P. Warnicke, P. Wohlhuter, J. M. George, M. Weigand, J. Raabe, V. Cros, and A. Fert, *Additive interfacial chiral interaction in multilayers for stabilization of small individual skyrmions at room temperature*. Nat. Nanotechnol. **11**, 444 (2016).

[49] K. O. Ng and D. Vanderbilt, *Stability of Periodic Domain-Structures in a 2-Dimensional Dipolar Model*. Phys. Rev. B **52**, 2177 (1995).

[50] A. C. Torrezan, J. P. Strachan, G. Medeiros-Ribeiro, and R. S. Williams, *Sub-nanosecond switching of a tantalum oxide memristor*. Nanotechnology **22**, 485203 (2011).

Figures

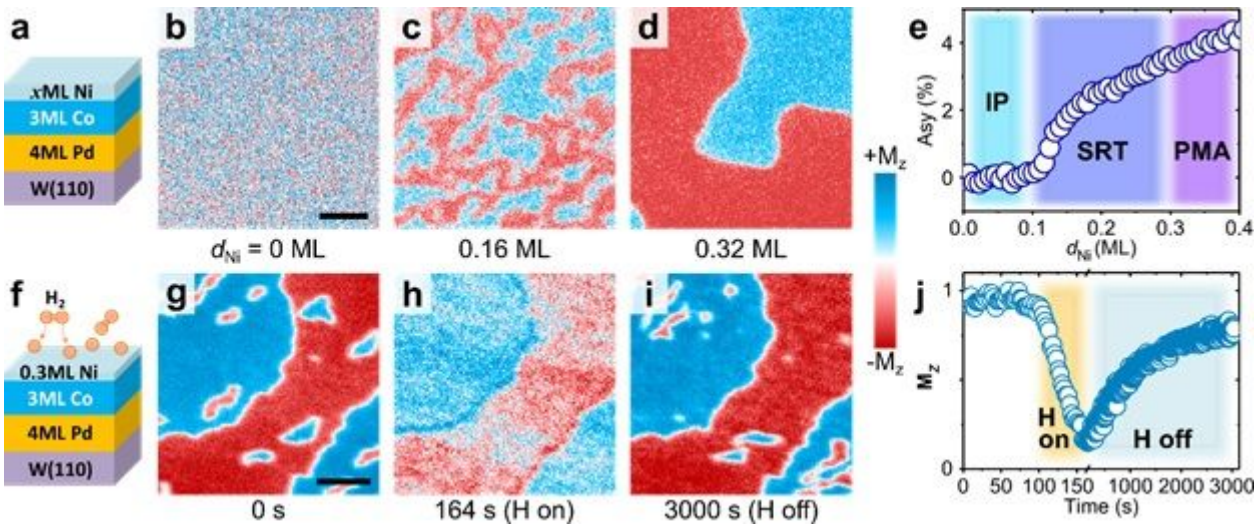

Figure 1

Hydrogen-induced magnetic anisotropy on NiCoPdW system. a, sketch of the sample structure. b-d, Ni thickness dNi dependent SPLEEM images with out-of-plane sensitivity in Ni/3ML Co/4ML Pd/W(110) system, showing evolution of perpendicularly magnetized domains. Scale bar 1μm. e, dNi dependent electron reflectivity spin-asymmetry of perpendicularly magnetized domains. IP, SRT, PMA stand for in-plane, spin reorientation transition and perpendicular magnetic anisotropy, respectively. f-i, hydrogen induced evolution of domains with out-of-plane sensitivity. Scale bar 1μm, indicating in-plane anisotropy induced by ~0.7 Langmuir hydrogen on 0.3ML Ni/3ML Co/4ML Pd/W(110) (panels g and h), and recovered perpendicularly magnetized domains upon hydrogen desorption (panel i). j, Time-dependent switching of out-of-plane magnetization (Mz) in one hydrogen on/off cycle.

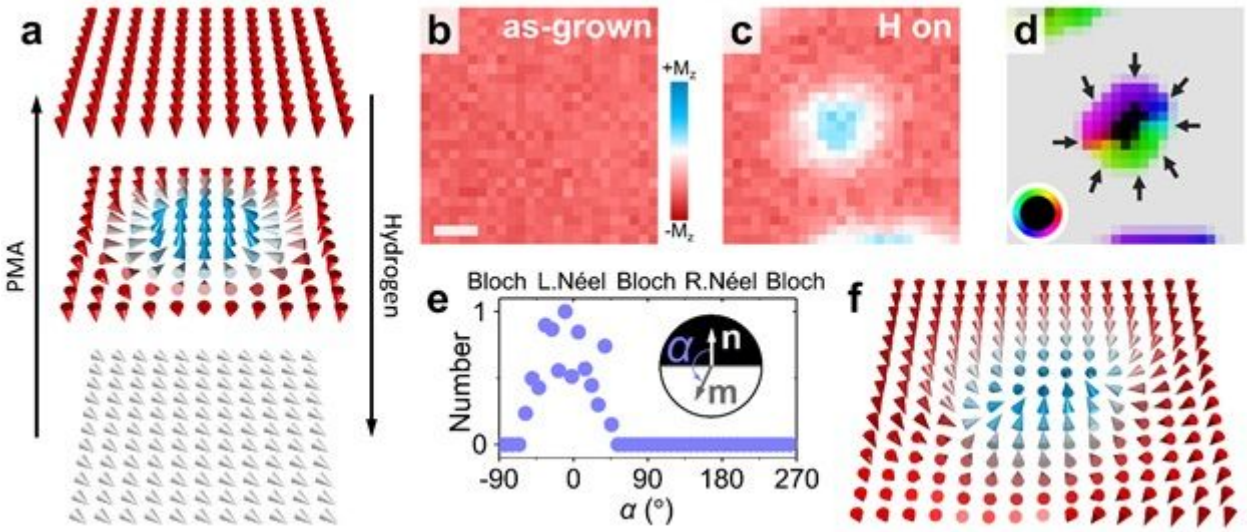

Figure 2

Hydrogen-induced skyrmion writing. a, perspective sketches of magnetization near spin reorientation transition in NiCoPdW(110). b, SPLEEM image of NiCoPdW(110) (near SRT) on a local -M_z domain. Scale bar is 100 nm. c, SPLEEM image at the same place as in panel b after 0.9 Langmuir hydrogen exposure, showing a bubble-like domain with +M_z. d, Compound SPLEEM image resolving the bubble-like domain as a skyrmion. Black/light grey represent up/down magnetization of the perpendicularly magnetized domains, respectively, and colour wheel shows in-plane magnetization direction within domain walls (also shown by black arrows). e, Histogram of angle α between magnetization m and boundary normal n, measured pixel-by-pixel along domain boundaries, indicating right-handed chiral Néel walls. f, Arrows-array representation of the skyrmion structure over a 200×200〖 nm〗^2 area, each arrow shows the magnetization vector direction of one pixel in panel d.

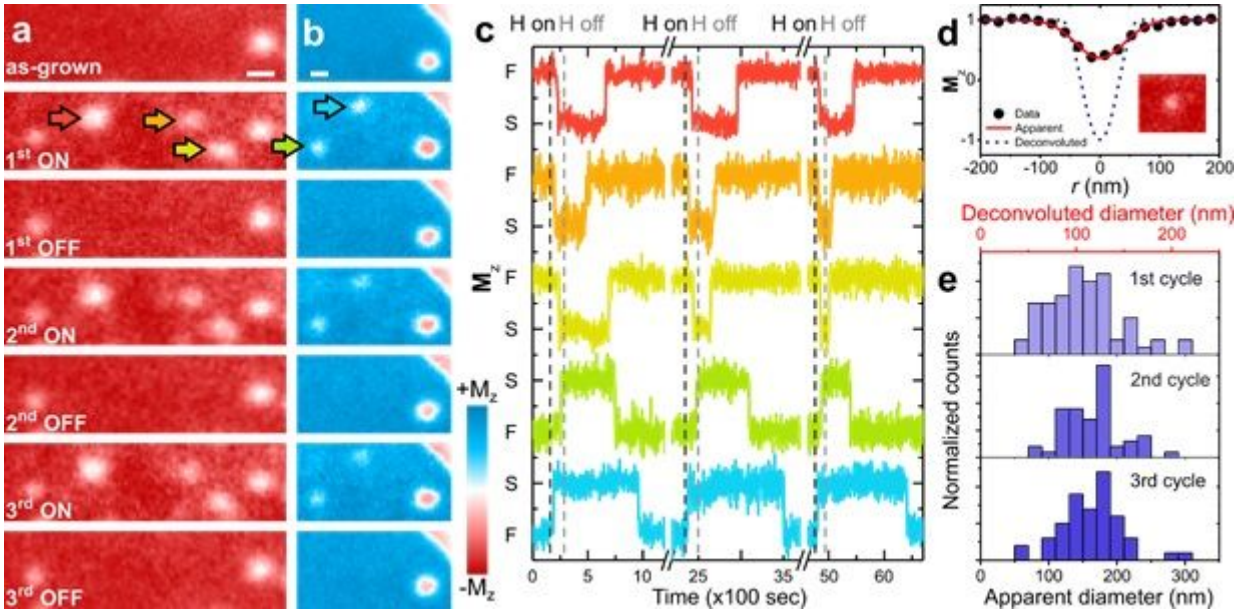

Figure 3

Reversible writing/deleting of magnetic skyrmions. a, SPLEEM images of perpendicularly magnetized domains in NiCoPdW(110), showing reversible skyrmion writing/deleting over three hydrogen on/off cycles (indicated by the red, orange and yellow arrows), scale bar is 200 nm. b, Similar time sequence as panel a, here on a +Mz domain (blue), showing reversible writing/deleting of two skyrmions (green and blue arrows), scale bar is 200 nm. c, Time-dependent Mz evolution at the centre of skyrmions highlighted by the arrows in panels a and b over three hydrogen ON/OFF cycles, showing reversible skyrmion switching between ferromagnetic state (F on y axis) and skyrmion state (S on y axis). Colour of the curve corresponds to the arrow colour. d, Mz profile of a skyrmion (see inset) and its deconvoluted profile in ideal imaging condition. e, Histograms of skyrmion diameters (lower scale image-apparent, upper scale deconvoluted measurements) over three cycles of H ON/OFF.

Figure 4

Monte-Carlo simulation of reversible writing/deleting of skyrmions via anisotropy change near SRT. a, Sketch of the anisotropy landscape, highlighting pinning sites with various magnetic anisotropy (labeled on top). b, Simulated domains over three anisotropy change cycles, showing reversible writing/deleting of

skyrmions on the sites with Kz=0.29, 0.27, 0.25 and 0.23. The amount of anisotropy change is indicated as ΔKz. c, Anisotropy dependent single-domain (open circles) and skyrmion (grey circles) evolution, summarizing panel b.

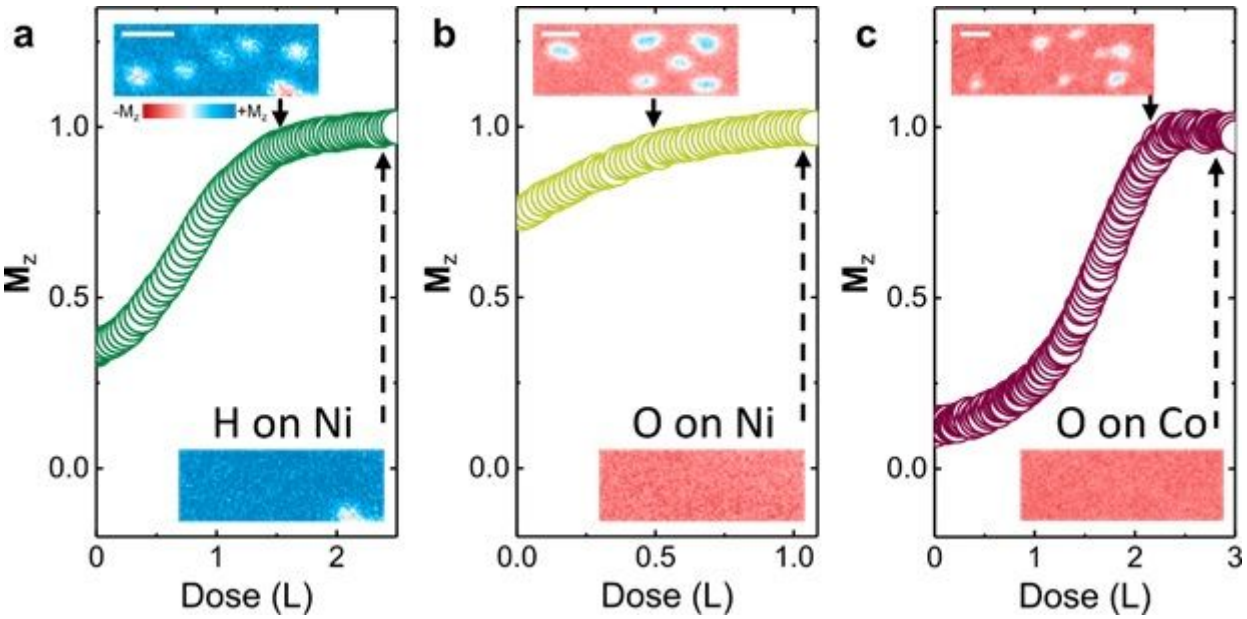

Figure 5

The role of chemisorbed hydrogen and oxygen on magnetic anisotropy and skyrmions on surfaces of other magnetic layers. a, Hydrogen induced anisotropy change (Mz) and skyrmion deleting (inserts) on surface of 2ML Ni/3ML Co/x ML Pd/W(110). The hydrogen pressure is 1.5 x 10-8 torr. The scale bar in the insert is 500 nm. b and c, Oxygen induced anisotropy change (Mz) and skyrmion deleting (inserts) on surface of 2ML Ni/3ML Co/x ML Pd/W(110) (panel b) and 0.1ML Ni/3ML Co/x ML Pd/W(110) (panel c). Scale bars in the inserts are 500 nm. The oxygen pressure is 2 x 10-9 torr in panel b and 1 x 10-8 torr in panel c.

Supplementary Files

This is a list of supplementary files associated with this preprint. Click to download.

- Supplementarymaterialsfinal.docx